Depth profiling of residual activity of ^{237}U fragments as a range verification technique for ^{238}U primary ion beam

I. Strašík,[1] V. Chetvertkova,[1,2] E. Mustafin,[1] M. Pavlovič,[3] and A. Belousov[1,4]

[1]*GSI Helmholtzzentrum für Schwerionenforschung, Planckstrasse 1, D64291 Darmstadt, Germany*
[2]*IAP Goethe Universität Frankfurt am Main, Max-von-Laue-Strasse 1, D-60438 Frankfurt am Main, Germany*
[3]*FEI STU, Ilkovičova 3, SK-81219 Bratislava, Slovak Republic*
[4]*Technische Universität Darmstadt, Karolinenplatz 5, D-64289 Darmstadt, Germany*

(Received 18 October 2011; published 3 July 2012)

Experimental and simulation data concerning fragmentation of ^{238}U ion beam in aluminum, copper, and stainless-steel targets with the initial energy 500 and 950 MeV/u are collected in the paper. A range-verification technique based on depth profiling of residual activity is presented. The irradiated targets were constructed in the stacked-foil geometry and analyzed using gamma-ray spectroscopy. One of the purposes of these experiments was depth profiling of residual activity of induced nuclides and projectile fragments. Among the projectile fragments, special attention is paid to the ^{237}U isotope that has a range very close to the range of the primary ^{238}U ions. Therefore, the depth profiling of the ^{237}U isotope can be utilized for experimental verification of the ^{238}U primary-beam range, which is demonstrated and discussed in the paper. The experimental data are compared with computer simulations by FLUKA, SRIM, and ATIMA, as well as with complementary experiments.

DOI: 10.1103/PhysRevSTAB.15.071001 PACS numbers: 25.70.Mn, 29.30.Kv, 24.10.Lx

I. INTRODUCTION

In the frame of the facility for antiproton and ion research (FAIR) project [1], activation of some accelerator construction materials by heavy-ion beams was studied at GSI Darmstadt with the aid of dedicated irradiation experiments [2–6] and computer simulations [7–9]. The goals of this research were to identify the nuclides induced in the irradiated materials including radioactive projectile fragments, to measure and calculate their partial residual activities (the partial residual activity is defined as the activity corresponding to a single nuclide), to measure depth profiles of the partial residual activities and to validate some computer codes used for simulation of interaction of high-energy ion beams with matter. The final goal was to specify tolerable beam losses in high-power heavy-ion machines [9].

The depth profiles of the partial residual activities were obtained from gamma spectra of individual activation foils contained in the target assembly (so-called stacked-foil geometry). In the case of ^{238}U primary beam, the ^{237}U isotope with a half-life of 6.75 days [10] was identified in all irradiated materials [2–4]. This isotope is a fragment of ^{238}U primary ion. Because the range of heavy ions at the same initial energy per nucleon is roughly proportional to A/Z^2 (A is the mass number and Z is the proton number of the ion), the ^{237}U fragments are expected to have the range very close to the range of the ^{238}U primary ions regardless of the depth where the fragmentation event occurs. A similar approach is used in ion therapy for verification of the spatial distribution of irradiating ions inside the patient body. For example, when ^{12}C ion beam is used for therapy, the ^{11}C isotope with half-life of 20.39 min is generated by projectile fragmentation. Since it is a positron emitter, its spatial distribution, which correlates to the distribution of the primary ^{12}C ions, can be imaged using positron emission tomography (PET) [11,12].

These facts motivated us to study a possibility of using depth profiling of the ^{237}U isotope as a range-verification technique for ^{238}U primary beam [13,14]. Results of this study are presented and analyzed in this paper. The study was performed by comparing results obtained from our activation (depth-profiling) experiments with computer simulations as well as with complementary experiments based on different techniques [15–17]. The computer simulations were performed with FLUKA [18–20], SRIM [21,22], and ATIMA [23]. The complementary experiments were based on dE/dx measurements [15] and beam tracking in an organic material [16,17].

II. EXPERIMENT AND METHODS

A. Targets and irradiation conditions

Eight targets assigned from T1 to T8 were irradiated with ^{238}U beam with the initial energy 500 MeV/u (T1, T2) and 950 MeV/u (T3–T8). Material of the T1–T4 targets was 99.5% natural aluminum ($\rho = 2.7$ g/cm^3). The T5 and T6 targets were made of 99.9% natural copper ($\rho = 8.92$ g/cm^3). The T7 and T8 target material was

austenitic stainless-steel type 304 ($\rho = 7.9$ g/cm^3). The assumed stainless-steel composition was (in weight fractions): C (0.08%), Mn (2.0%), P (0.045%), S (0.03%), Si (0.75%), Cr (18%–20%), Ni (8%–10.5%), and N (0.1%) in addition to iron. The targets were cylinders assembled from many individual foils of various thicknesses (stacked-foil targets). The diameter of the T1–T5 and T7 targets was 50 mm. The diameter of the T6 and T8 targets was 25 mm. The thin activation foils (about 100 μm) were placed in the region of the expected range of the ^{238}U primary ions. The range of the primary ions was preestimated using computer simulations and complementary experiments [15–17].

^{238}U beams from the SIS-18 synchrotron at the GSI Darmstadt were used to irradiate the targets at two different nominal energies of 500 and 950 MeV/u. The nominal energies are the energies set for the extraction from the synchrotron. According to the experience of the SIS18 operation crew and the machine coordinator, the momentum deviation can be of the same order as momentum spread of the beam. For the momentum spread of the beam, dp/p, the value of 5×10^{-4} (1σ) was recommended to us by the SIS-18 operation team based on the data used for beam-transport simulations and by the SIS18 control system. Nevertheless, we performed simulations for three different levels of momentum spread: 2.5×10^{-4}, 5×10^{-4}, and 7.5×10^{-4} representing $\pm 50\%$ deviation from the recommended value. The momentum spread does not influence the beam range; it influences the range straggling only (detailed numerical values will be presented below).

The aluminum targets were irradiated in the fast-extraction regime with cycle duration of 3 s. The beam spot size was about 2 cm in the horizontal plane and 2 cm in the vertical plane (checked visually on a scintillation screen and measured using a profile meter). The beam profile was approximately Gaussian according to the profile meter. The beam intensity was monitored using a current transformer [24]. The copper and stainless-steel targets were irradiated in the slow-extraction regime with a repetition rate of 0.285 Hz (3.51 s per cycle) and spill duration of 1 s. The beam spot size was about 8 mm in diameter as observed visually on the scintillation screen immediately before irradiation. The beam profile was also approximately Gaussian according to the profile meter. The beam intensity was monitored using the secondary electron transmission monitor (SEETRAM) [25].

The irradiation conditions and total numbers of ions delivered to the targets are summarized in Table I. The initial energy of the primary beam presented in the table stands for the nominal energy of the synchrotron. In the experiments performed with the aluminum targets (T1–T4, fast extraction, beam intensity monitored by the current transformer), the primary particles lost a small amount of energy in a 100 μm thick vacuum window made of stainless steel and in 1 m long air drift space between the end of the beam pipe and the target. In the experiments performed with the copper and stainless-steel targets (T5–T8, slow extraction, beam intensity monitored by the SEETRAM), the primary particles lost a small amount of energy in the 100 μm thick vacuum window made of aluminum, 64 cm long air drift space and three SEETRAM titanium foils each 10 μm thick.

The targets were irradiated in four different beam-time slots: T1 and T3 in the first beam time, T2 and T4 in the second one, T5 and T7 in the third one, and T6 and T8 in the fourth one. The beam-time slots were separated by several months from each other.

B. Measurements of gamma spectra

After the end of irradiation, the gamma spectra of the activation foils were measured. The first measurement started a few hours after the end of irradiation and the last measurement was performed several days after the end of irradiation. The time-slot for measurements is limited by the half-life of the ^{237}U isotope (6.75 days). The spectrum-acquisition time varied from a few minutes up to several hours per foil. The foil-to-detector distance was 7 cm.

The gamma-ray spectroscopy measurements were carried out with the Canberra HPGeGC3518 and Ortec GEM25P4 detectors coupled to Silena multichannel analyzers (8192 channels) and the Ortec GEM20P4 detector coupled to an Ortec multichannel analyzer (also 8192 channels). The detectors were powered by an Ortec high voltage supply. For the energy and efficiency calibration, a set of calibration sources was used: ^{22}Na, ^{60}Co, ^{133}Ba, ^{137}Cs, ^{152}Eu, ^{210}Pb, and ^{241}Am. Data acquisition and handling of spectra were controlled by the Wingam and GammaVision-32 software packages. The spectra were analyzed using the GammaVision-32 and Genie2000 software packages.

Decay of ^{237}U is accompanied by emission of several gamma rays with various energies. The gamma rays with emission probability per one decay over 1% are: 26.3 keV

TABLE I. Irradiation conditions and total numbers of ions delivered to the targets.

Target	T1	T2	T3	T4	T5	T6	T7	T8
Target material	Al	Al	Al	Al	Cu	Cu	Steel	Steel
Initial beam energy [MeV/u]	500	500	950	950	950	950	950	950
Number of ions	4.1×10^{11}	1.6×10^{12}	5.1×10^{11}	8.4×10^{12}	8.0×10^{10}	8.3×10^{9}	8.7×10^{10}	2.1×10^{10}

(2.43%), 59.5 keV (34.5%), 64.8 keV (1.3%), 164.6 keV (1.9%), 208.0 keV (21.2%), and 332.4 keV (1.2%) [10]. Among these gamma rays, the 208.0 keV gamma spectral line is best suited for calculation of the ^{237}U activity for several reasons: (1) there is no interference with gamma lines of other nuclides induced in the target, (2) its gamma-ray emission probability is high enough, and (3) detection efficiency is high for photon energies around 200 keV. The 59.5 keV gamma line was not used for cross-checking of the measured activities because it suffers from an interference with other nuclides. The signal from other gamma lines was too low for cross-checking and there was also an indication of the interference with other nuclides. Nevertheless, the 208 keV gamma line was cross-checked by repeated measurements of the samples.

C. Range and methods of range calculation

The range can be defined and interpreted in several ways. The so-called continuous slowing-down approximation range is expressing the total path length needed to lose all of the particle's kinetic energy. This range is defined by the formula

$$R_{\text{total}} = \int_0^{E_0} \left(\frac{dE}{dx}\right)^{-1} dE, \tag{1}$$

where E_0 is the particle kinetic energy at the target surface and dE/dx is the average unrestricted stopping power.

This definition is—from the point of view of practical applications and experimental verification—of less concern. The particle trajectory inside a material has a complicated shape and its total length can hardly be measured. For experimental verification, another possible definition, the projected range, R_p is more important. Projected range is defined as an average value of the depth to which a charged particle will penetrate in the course of slowing down to rest. This quantity can be calculated from data obtained by Monte Carlo simulations as the mean value of individual projected ranges [21]:

$$R_p = \langle x \rangle = \frac{1}{N} \sum_{j=1}^{N} x_j, \tag{2}$$

where x_j is the projected range of the jth ion and N is the total number of ions.

Although this definition can be applied generally to any initial beam direction, in our experiments the beams irradiated the targets perpendicularly to the target surface, hence the x direction (target depth) is aligned with the incoming-beam direction. For simplicity, this "projected range" will be referred to as "range" through further text in this paper.

Variance, σ^2, is the second moment of the range distribution:

$$\sigma^2 = \langle (x - R_p)^2 \rangle = \frac{1}{N} \sum_{j=1}^{N} (x_j - R_p)^2 = \langle x^2 \rangle - \langle x \rangle^2. \tag{3}$$

Range straggling, σ, is commonly defined as the square root of the variance [21].

In case of depth-profiling experiments, the depth resolution is limited by the final thickness of the activation foils and the range distribution becomes a histogram of number of particles that stopped in a particular activation foil. The number of radioactive nuclides, n_i, that stopped in the ith foil can be obtained by measuring its partial activity in the ith foil, a_i, thanks to the relation

$$a_i = \lambda n_i, \tag{4}$$

where λ is the decay constant.

Definitions (2) and (3) have to be adapted accordingly. Let us assume the situation according to Fig. 1.

The depth-profiling experiment yields the range-distribution histogram that can be interpreted as a stepwise sample probability density function, $f(x)$, defined as

$$f(x) = f_i(x) = \frac{n_i}{N(L_{i,2} - L_{i,1})} \quad \text{for } L_{i,1} \le x < L_{i,2}, \tag{5}$$

where n_i is the number of particles that stopped in the ith foil, N is the total number of particles, and $L_{i,1}$ and $L_{i,2}$ are the front and end position of the ith activation foil, respectively. Probability, p_i, that a particle stops in the ith foil will be

$$p_i = \int_{L_{i,1}}^{L_{i,2}} f_i(x)dx = \frac{n_i}{N} = \frac{a_i}{A_\Sigma}, \tag{6}$$

where A_Σ is the sum of activities of all activation foils.

The range, R_p, can be calculated as the mean value of the range distribution:

$$R_p = \int_0^\infty x f(x) dx. \tag{7}$$

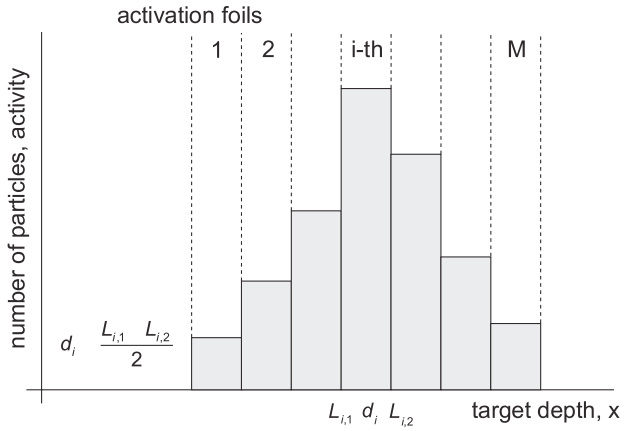

FIG. 1. A schematic range distribution as measured by a depth-profiling experiment.

Performing this integration in a stepwise manner for all activation foils (M is the total number of activation foils) yields

$$R_p = \sum_{i=1}^{M}\left[\int_{L_{i,1}}^{L_{i,2}} x f_i(x)dx\right] = \sum_{i=1}^{M}\left[\frac{(L_{i,2}+L_{i,1})}{2}\frac{n_i}{N}\right] = \sum_{i=1}^{M}[d_i p_i]. \quad (8)$$

This means that each activation foil can be represented by the position of its center, d_i, and the probability that a particle stops in the foil, $p_i = n_i/N = a_i/A_\Sigma$. Such a simplification is no longer possible for the variance that becomes

$$\sigma^2 = \int_0^\infty (x-R_p)^2 f(x)dx = \sum_{i=1}^{M}\left[\frac{((L_{i,2}-R_p)^3-(L_{i,1}-R_p)^3)}{3(L_{i,2}-L_{i,1})}p_i\right]. \quad (9)$$

III. COMPUTER SIMULATIONS

Computer simulations provided range estimation for the proper target arrangement (the thin activation foils must be positioned in the range region of ^{237}U ions), information about the differences between the range of ^{238}U primary ions and ^{237}U fragments, as well as data to be validated with experimental results. Three codes were used for simulations: FLUKA2011.2.3 [18–20], SRIM2011.06 [21,22], and ATIMA1.2 [23]. These codes differ by the level of complexity and by physical phenomena that are (or that are not) included in the underlying physical models.

ATIMA is a computer code that—among others—calculates the following physical quantities related to interaction of ions with matter: stopping power, energy loss, energy-loss straggling, angular straggling, range and range straggling for kinetic energies from 1 keV/u to 450 GeV/u [23]. Above 30 MeV/u the stopping power is obtained from the Lindhard and Soerensen theory [26]. This theory is based on a precise quantum mechanical calculation of the energy transfer in the interaction process of projectiles with target electrons. Essential is to calculate the deviation of the precise theory from the first-order quantum perturbation. This deviation can be expressed in terms of the transport cross section for scattering of a free electron by the ion [26]. The shell corrections, the Barkas effect, the Bloch correction, and the Fermi density effect are included in the calculation. Projectiles are treated as ions with the size of the nucleus with a mean charge. It also considers the nuclear size effect for relativistic ions. Below 10 MeV/u an older version of Ziegler's SRIM is used [27]. In the intermediate energy range, an interpolation between the two approaches is used.

Stopping and range of ions in matter (SRIM) is more complex than ATIMA. Its physics is thoroughly described in Refs. [21,22]. SRIM simulates interaction of ions with matter with initial kinetic energies from 10 eV/u to 2 GeV/u. It uses several different stopping theories. For high-energy heavy ions, which is the case of our present study, the stopping power has two components related to: (a) charge state of the ions (Brandt-Kitagawa approximation [28]) and (b) the component described by the Bethe formula [21,22]. The formula contains the mean ionization potential, the shell corrections, the density effect as well as the Barkas and Bloch correction terms [21]. The parameters of the formulas are optimized by weighting with experimental data [21,22]. SRIM calculations can be done using two separate modules: (a) stopping/range tables and (b) transport of ions in matter (TRIM), both using the same stopping powers. SRIM takes into account merely elastic nuclear collisions and inelastic electronic collisions. Inelastic nuclear collisions are not considered. This means in our particular case that production of the projectile fragments along the projectile path cannot be simulated.

In the stopping/range tables module, the elastic collisions between the ion and the target nuclei cause both angular deflections and stopping of the ion. The inelastic collisions with the target electrons are treated as a continuous slowing-down process. The stopping/range tables module generates quickly tables of the stopping powers (nuclear and electronic stopping powers are listed extra), projected range, longitudinal straggling, and lateral straggling as a function of the initial ion energy. The range is calculated by solving the transport equation using the so-called projection range algorithm (PRAL) [21]. The PRAL ranges are usually within 5% of those obtained with the TRIM Monte Carlo module.

The TRIM module uses the Monte Carlo approach. In this case, more output quantities like damage events, ionization profiles, sputtering yield, etc. are calculated in addition to the range and range straggling. The Monte Carlo module allows also simulating of interaction of ions with multilayer targets using a quantum mechanical treatment of individual collisions. The primary ion and the target atom are assumed to have a screened Coulomb collision including exchange and correlation between the overlapping electron shells. The charge state of the ion is described using the effective-charge concept, which includes a velocity dependent charge state and long-range screening due to the collective electrons of the target [21].

FLUKA is a multipurpose Monte Carlo software package for simulation of interaction and transport of different particles in matter. The particle species include photons, electrons, neutrinos, muons, hadrons, antiparticles, neutrons, and ions up to TeV energies. It has variety of applications in high-energy physics, radiation protection, detector and telescope design, cosmic-ray studies, dosimetry, engineering, medical physics, and radiobiology. The FLUKA physical models are described in Refs. [18,19]. In contrast to ATIMA and SRIM, FLUKA does include inelastic

nuclear interactions. They are treated through interfaces to external event generators. There are DPMJET-II or DPMJET-III (dual parton) models for energies above 5 GeV/u, modified relativistic quantum molecular dynamics model for energies from 0.125 GeV/u to 5 GeV/u, and Boltzmann master equation model for energies below 0.125 GeV/u. The stopping power of charged particles is calculated using the Bethe-Bloch theory with the following parameters involved: mean excitation energy (material dependent), density correction, shell correction, and maximum energy transfer to an electron [20]. There are also higher-order corrections implemented: Barkas correction, Bloch correction, and Mott corrections. Effective-charge parametrizations are implemented for heavy ions. Above a preset threshold, ionization is modeled as δ-rays production. In this process an electron is ejected from an atom with sufficient energy to cause secondary ionization. The threshold refers to the kinetic energy of the emitted δ ray. Below the δ-ray threshold, energy losses are treated as "continuous" with some special features. Besides Coulomb scattering with atomic electrons, particles undergo Coulomb interaction also with atomic nuclei. The nuclear stopping power is smaller than the electronic one, but is important for heavy ions [20]. The electromagnetic dissociation (EMD) [29–31] can be activated.

For the range calculation, the evaluation of stopping powers is of crucial importance. This concerns all three codes used in our study. The state-of-the-art analysis of this problem can be found in [32] and numerous references therein. It should be noted that, as far as the mean ionization potential is concerned, we always used the default values as implemented in the above-mentioned codes.

A. SRIM and ATIMA simulations

In order to get a quantitative assessment of the difference between the ^{237}U and ^{238}U range, first computer simulations were done with SRIM and ATIMA, which are less complex and less time consuming than FLUKA. Because the range of ions at the same kinetic energy per nucleon is roughly proportional to A/Z^2, the range of the ^{237}U fragments is expected to be slightly shorter than the range of the ^{238}U primary ions. The largest difference between the ^{237}U-ion and ^{238}U-ion ranges corresponds to the situation when a fragmentation event occurs at the target surface. This can be simulated by SRIM and ATIMA using ^{237}U and ^{238}U primary beams. Results are collected in Table II. The SRIM simulations were performed with the TRIM Monte Carlo module. The difference between the range of the ^{237}U and ^{238}U primary ions is less than 0.5% in all cases. The largest difference is in aluminum at 950 MeV/u corresponding to the longest range. The range straggling is almost identical for both primary beams in all targets.

Although these simulations are rather simplified, they confirm the assumption that the difference between the ^{237}U-ion and ^{238}U-ion ranges (even in the limit case of the fragmentation event at the target surface) is small. It is less than 0.5%, which supports the idea of using the ^{237}U depth profiling as a range-verification technique for ^{238}U beam.

B. FLUKA simulations

The most realistic simulations can be done with FLUKA that does take into account inelastic nuclear collisions including the fragmentation (in contrast to SRIM and ATIMA). Thanks to that, transport of the ^{238}U primary ions including the fragmentation process resulting in generation of the ^{237}U fragments and their subsequent transport can be simulated. Another advantage is that FLUKA allows us to introduce a momentum spread of the incident beam. In the FLUKA simulations, the heavy-ion transport with nuclear interactions was switched on. The electromagnetic dissociation (EMD) was activated for primary ions as well as for target nuclei. The new evaporation model with heavy-fragment evaporation was used. Emission of the high-energy light fragments through the coalescence mechanism was also activated.

The calculated range and the range straggling are presented in Table III. Corresponding simulated depth profiles

TABLE II. Range and range straggling of the ^{237}U and ^{238}U beams in aluminum, copper, and stainless-steel targets calculated by SRIM2011.06 (Monte Carlo module TRIM) and ATIMA1.2. In these calculations, both isotopes were transported as primary ions. The initial energy of the primary ions was 500 and 950 MeV/u, no momentum spread. Energy losses of the primary beam in the vacuum window, air gap, and SEETRAM were taken into account.

Target material		Aluminum	Aluminum	Copper	Stainless steel
Initial beam energy [MeV/u]		500	950	950	950
On-target beam energy [MeV/u]		485 (SRIM) 483 (ATIMA)	937 (SRIM) 935 (ATIMA)	942 (SRIM) 941 (ATIMA)	942 (SRIM) 941 (ATIMA)
		Range ± range straggling [mm]			
SRIM (TRIM)	^{237}U	16.10 ± 0.02	41.24 ± 0.04	14.57 ± 0.02	15.61 ± 0.02
	^{238}U	16.19 ± 0.02	41.41 ± 0.04	14.64 ± 0.02	15.68 ± 0.02
ATIMA	^{237}U	15.15 ± 0.01	37.41 ± 0.03	12.86 ± 0.01	14.26 ± 0.01
	^{238}U	15.22 ± 0.01	37.57 ± 0.03	12.91 ± 0.01	14.32 ± 0.01

TABLE III. Range and range straggling of the ^{237}U fragments and the ^{238}U primary ions in aluminum, copper, and stainless-steel target calculated by FLUKA2011.2.3. The initial energy of the primary ions was 500 and 950 MeV/u. Energy losses of the primary beam in vacuum window, air gap, and SEETRAM and 1σ-momentum spread of the beam $dp/p = 5 \times 10^{-4}$ were taken into account in the calculations. The relative standard uncertainty of the presented data is below 1%.

Target material		Aluminum	Aluminum	Copper	Stainless steel
Initial beam energy [MeV/u]		500	950	950	950
On-target beam energy [MeV/u]		483	937	942	942
		Range ± range straggling [mm]			
FLUKA	^{237}U	14.96 ± 0.04	37.33 ± 0.08	13.01 ± 0.03	14.08 ± 0.03
	^{238}U	15.00 ± 0.03	37.43 ± 0.05	13.04 ± 0.02	14.11 ± 0.02

of the residual activity of both uranium isotopes are shown in Fig. 2.

The difference between the range of ^{237}U and ^{238}U is even smaller than in the case of ATIMA and SRIM simulations. However, the range straggling of the ^{237}U fragments calculated by FLUKA is from about one and a half to two times larger than the range straggling of the ^{238}U primary ions. This is, naturally, caused by the fact that the fragmentation events occur in different depths of the target, which also shifts the ^{237}U range towards the ^{238}U range. In this case, the stopping point of a ^{237}U fragment is indicating the ^{237}U range containing a part of the trajectory from the target surface to the position where the fragmentation event occurred. This part was, however, traveled not by the ^{237}U fragment but by its parent ^{238}U primary ion. The range straggling (for both isotopes) is also enhanced by the initial momentum spread of the incoming beam. Whereas the SRIM and ATIMA simulations were done for monoenergetic beams, the FLUKA simulations were done for three different levels of momentum spread: the reference value of 5×10^{-4} plus 2.5×10^{-4} and 7.5×10^{-4} representing ±50% deviation from the reference one. Momentum spread does

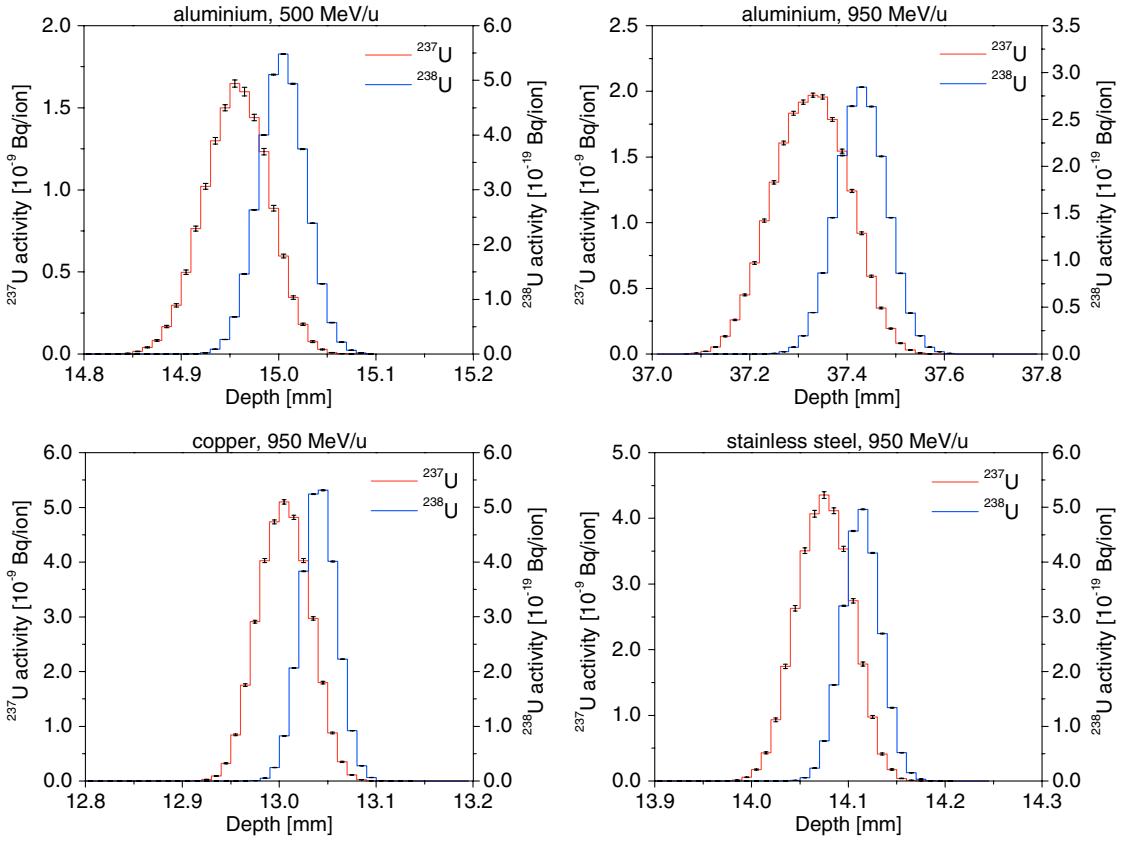

FIG. 2. Depth profiles of the residual activity of the ^{238}U primary ions and the ^{237}U fragments in aluminum, copper, and stainless-steel target simulated using FLUKA2011.2.3. The initial energy of the primary ions was 500 and 950 MeV/u. The depth resolution of simulated profiles is 10 μm (aluminum irradiated with 500 MeV/u beam, copper irradiated with 950 MeV/u beam, and stainless steel irradiated with 950 MeV/u beam) and 20 μm (aluminum irradiated with 950 MeV/u beam).

not influence the range and its influence on the range straggling for copper target irradiated with 950 MeV/u (as an example) was the following. For ^{238}U, the simulated range straggling was 0.015, 0.019, and 0.024 mm for $dp/p = 2.5 \times 10^{-4}$, 5×10^{-4}, and 7.5×10^{-4}, respectively. For ^{237}U, the simulated range straggling was 0.024, 0.026, and 0.029 mm for $dp/p = 2.5 \times 10^{-4}$, 5×10^{-4}, and 7.5×10^{-4}, respectively. It becomes clear that accuracy of the momentum-spread determination is not crucial for our study.

The activity of the ^{238}U (normalized per one incident ion) is about 10 orders of magnitude lower than the activity of the ^{237}U (see Fig. 2). This is due to much longer half-life of the ^{238}U (4.468×10^9 years) compared with the half-life of the ^{237}U (6.75 days) [10]. Production of the ^{237}U fragments per one incident ion is lower than conservation of the ^{238}U projectiles by 1 order of magnitude (see Table IV).

Conservation of the ^{238}U projectiles is the lowest in case of the aluminum irradiated with the 950 MeV/u primary beam. The mean-free path for nuclear interaction in copper and stainless steel is about twice shorter than in aluminum [9,33]. On the other hand, the range of the ^{238}U beam at 950 MeV/u in aluminum is almost 3 times longer than in copper or stainless steel as well as the range of the ^{238}U beam at 500 MeV/u in aluminum (see Tables II and III). For this reason, the probability of nuclear interaction is the highest in the case of aluminum irradiated by ^{238}U beam with initial energy 950 MeV/u, which results in the lowest number of the ^{238}U projectiles in this target. Production of the ^{237}U fragments is the highest for the copper irradiated with the 950 MeV/u primary beam. This is very likely due to the electromagnetic dissociation (EMD) process that becomes important for nuclear interaction of high-energy heavy ions [29–31]. For single and few nucleons removal in nucleus-nucleus collision, EMD cross section is significantly increasing with increasing proton number of the target nuclei as well as with increasing proton number of the primary ions. It is also increasing with increasing energy of the projectiles [29–31]. That is why the highest number of the ^{237}U fragments is generated in the copper target irradiated with 950 MeV/u primary beam.

Conservation of the ^{238}U projectiles is the highest for the aluminum target irradiated with uranium beam with the initial energy 500 MeV/u. It is due to longer mean-free path for nuclear interaction in comparison with the mean-free path in copper and stainless steel [9,33], as well as shorter range of the projectiles with the initial energy 500 MeV/u. For these reasons, the probability of nuclear interaction is the lowest in this target. In the same target, production of the ^{237}U fragments is the lowest. Besides the low probability of nuclear interaction, it is also due to low EMD cross section for single and few nucleons removal in nucleus-nucleus collision.

IV. EXPERIMENTAL RESULTS

A. Depth profiling of the residual activity of ^{237}U

Depth profiles of the residual activity of ^{237}U were obtained using gamma spectroscopy of the thin activation foils from the range region of the primary ions. They are shown in Fig. 3. The activities are extrapolated to the end of irradiation and normalized per one incident ion. All depth profiles have a peaklike shape and occupy a region few hundreds μm thick. Distribution of ^{237}U in the aluminum targets at 950 MeV/u is slightly broader. In this case, the range of the ^{237}U fragments is by about a factor of 3 longer than in other cases. It can be seen that the absolute value of the ^{237}U activity is increasing with increasing proton number of the target material as well as with increasing energy of the primary ions (see also Sec. III B).

It should be noted that the profiles presented in Fig. 3 corresponding to the same material and the same beam energy were measured in different beam times separated from each other by several months and the same target material does not mean the same target. A new target was fabricated for the new beam time. Although the new targets were fabricated from the same raw material, the reproducibility of the target is still limited by mechanical tolerances of the fabrication process (target geometry) and possible inhomogeneities of the raw material. There are several other parameters that can never be perfectly reproduced in two independent experiments. The vacuum window terminating the beam pipe was exchanged between the two experiments at least once due to vacuum problems. Also its properties might be altered between the experiments. Moreover, air temperature, air pressure, and air humidity in the experimental cave might be different, the positioning of the sample with respect to the incoming beam can also be done with restricted reproducibility

TABLE IV. Production of the ^{237}U fragments and conservation of the ^{238}U projectiles per one incident ion in aluminum, copper, and stainless-steel target calculated by FLUKA2011.2.3. The initial energy of the primary ions was 500 and 950 MeV/u. The relative standard uncertainty of the presented data is below 1%.

Target material		Aluminum	Aluminum	Copper	Stainless steel
Initial beam energy [MeV/u]		500	950	950	950
		Number of isotopes per one incident ion			
FLUKA	^{237}U	1.16×10^{-2}	1.68×10^{-2}	2.93×10^{-2}	2.67×10^{-2}
	^{238}U	6.71×10^{-1}	3.72×10^{-1}	5.10×10^{-1}	4.97×10^{-1}

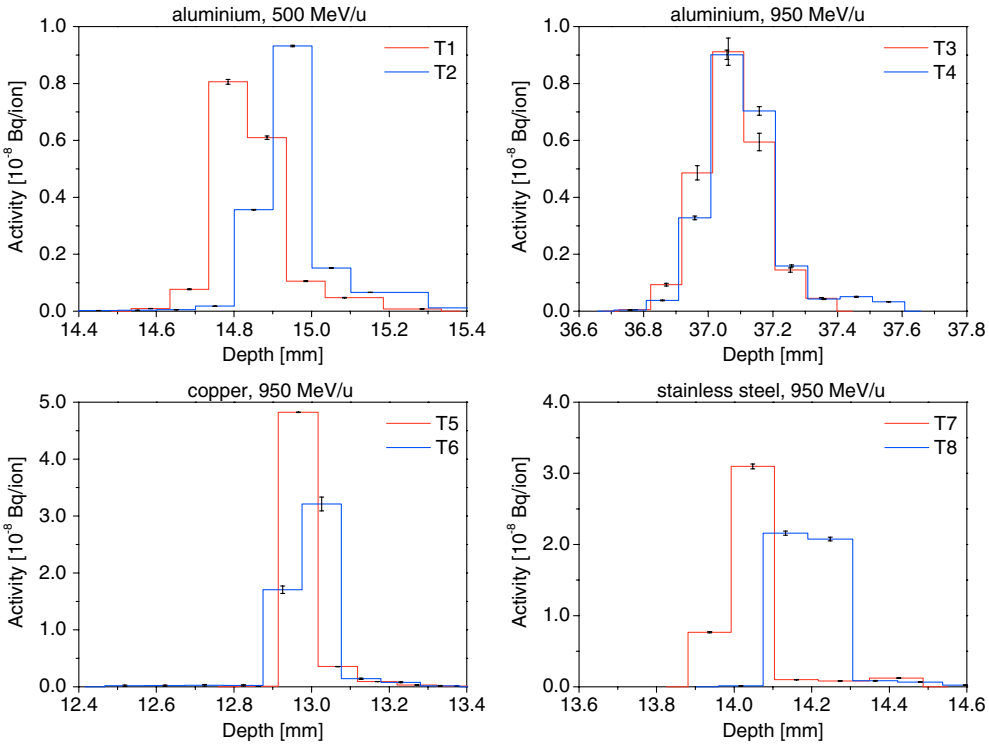

FIG. 3. Experimental depth profiles of the ^{237}U residual activity in the aluminum, copper, and stainless-steel targets irradiated with ^{238}U primary beam with the initial energy 500 and 950 MeV/u.

only, etc. That is why the agreement is not always excellent, but it is within the experimental uncertainty that is going to be evaluated in Sec. IV D.

B. Complementary experiments

A complementary experimental technique for range measurements is based on the fact that heavy ions create visible radiation damage to an organic foil manifested as darkening of the foil [16,17]. The darkest spot on the foil corresponds to the position of the energy-deposition maximum (the Bragg peak) that can be used as an estimate of range. We checked by computer simulations that the difference between the position of the Bragg peak and the mean range calculated according to Eq. (8) is much less than the experimental uncertainty. That is why the range of ions can be measured using a truncated cylinder covered by an organic foil on its bevelled side (see Fig. 4). We irradiated an aluminum cylinder with ^{238}U ion beam. Initial energies of the beam were 500 and 950 MeV/u. The primary particles again lose a small part of energy in 100 μm thick vacuum window made of stainless steel and in 1 m long air drift space between the end of the beam pipe and the target. The darkened regions on the foil are clearly visible (see Fig. 4, right) and were used to estimate the ^{238}U range in aluminum. The estimated values were 14.8 and 37.0 mm for the initial energy 500 and 950 MeV/u, respectively. The accuracy of this method is assumed to be $\pm$0.25 mm [16,17].

In the case of the copper and stainless-steel targets, data from a dE/dx experiment were adopted [15]. This experiment provides the range of 13.1 and 14.4 mm for copper and stainless steel, respectively irradiated with

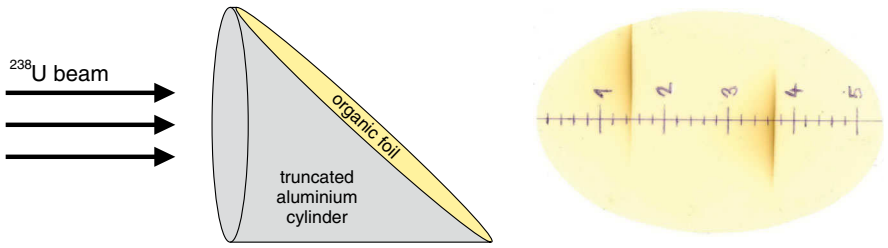

FIG. 4. Principal scheme of the complementary experiment using the truncated aluminum cylinder with an organic foil (left) and the corresponding darkened regions on the foil created with ^{238}U ions (right) with the initial energy 500 MeV/u (shorter range) and 950 MeV/u (longer range).

950 MeV/u ^{238}U ion beam. Accuracy of the range from the dE/dx experiment is ±0.4 mm.

C. Comparison of the results

The range and range straggling determined from depth profiling of the ^{237}U residual activity using Eqs. (8) and (9) are summarized in Table V together with data obtained from the computer simulations and the complementary experiments described above.

It can be seen from Table V that in most cases the best agreement is between experimental data and FLUKA simulations. SRIM overestimates the range in all targets and deviation is the largest compared with other simulation codes. ATIMA overestimates the range in the aluminum targets and the stainless-steel targets (except for the range determined from the dE/dx experiment). It underestimates the range in the copper targets, but the agreement is still satisfactory. It should also be noted that results obtained by different experimental techniques are well consistent. Because the final goal is to use the depth profiling of ^{237}U residual activity as a range-verification technique for the ^{238}U primary beam, Table VI contains relative deviations of the ^{237}U range obtained by the depth-profiling technique from ^{238}U ranges calculated by FLUKA or determined by complementary experiments. The deviations are quoted with respect to the depth-profiling experiment:

$$\partial = \frac{|R_{p,X} - R_{p,\mathrm{DP}}|}{R_{p,\mathrm{DP}}} 100\%, \tag{10}$$

where $R_{p,X}$ is the range of the ^{238}U primary beam simulated by FLUKA or determined by a complementary experiment and $R_{p,\mathrm{DP}}$ is the range obtained by depth profiling of the residual activity of the ^{237}U fragments.

D. Uncertainty assessment

The uncertainties were analyzed according to the International Organization for Standardization Guide to the Expression of Uncertainty in Measurement [34]. The standard uncertainty of the ^{237}U range [Eq. (8)] comprises the following components: (1) depth uncertainty, $u(d)$,

TABLE V. Range and range straggling of the ^{237}U fragments and the ^{238}U primary ions in aluminum, copper, and stainless-steel targets measured experimentally and calculated using computer codes. The energy of the primary beam presented in the table is the synchrotron nominal energy. Energy losses of the primary beam in vacuum window, air drift space, and SEETRAM are taken into account. In case of the FLUKA simulations and depth-profiling experiments, the range and the range straggling are calculated according to Eqs. (8) and (9), respectively. This range straggling does not take into account the uncertainties of the input quantities and must not be interpreted as the uncertainties of the presented data. The beam momentum spread in FLUKA simulations was 5×10^{-4} (1σ).

	^{237}U				^{238}U		
	Depth profiling	FLUKA	dE/dx	Organic foil	FLUKA	SRIM (TRIM)	ATIMA
	Range [mm] ± range straggling [mm]						
T1 Aluminum 500 MeV/u	14.84 ± *0.09*	14.96 ± *0.04*	···	14.8	15.00 ± *0.03*	16.19 ± *0.02*	15.22 ± *0.01*
T2 Aluminum 500 MeV/u	14.95 ± *0.10*	14.96 ± *0.04*	···	14.8	15.00 ± *0.03*	16.19 ± *0.02*	15.22 ± *0.01*
T3 Aluminum 950 MeV/u	37.08 ± *0.11*	37.33 ± *0.08*	···	37.0	37.43 ± *0.05*	41.41 ± *0.04*	37.57 ± *0.03*
T4 Aluminum 950 MeV/u	37.11 ± *0.13*	37.33 ± *0.08*	···	37.0	37.43 ± *0.05*	41.41 ± *0.04*	37.57 ± *0.03*
T5 Copper 950 MeV/u	12.98 ±*0.06*	13.01 ±*0.03*	13.1	···	13.04 ±*0.02*	14.64 ±*0.02*	12.91 ±*0.01*
T6 Copper 950 MeV/u	12.99 ± *0.09*	13.01 ± *0.03*	13.1	···	13.04 ± *0.02*	14.64 ± *0.02*	12.91 ± *0.01*
T7 Stainless steel 950 MeV/u	14.05 ± *0.09*	14.08 ± *0.03*	14.4	···	14.11 ± *0.02*	15.68 ± *0.02*	14.32 ± *0.01*
T8 Stainless steel 950 MeV/u	14.20 ± *0.09*	14.08 ± *0.03*	14.4	···	14.11 ± *0.02*	15.68 ± *0.02*	14.32 ± *0.01*

TABLE VI. Relative deviations between the uranium-beam ranges determined by different methods with respect to the range determined by the depth-profiling technique.

Target	Target material	Initial beam energy [MeV/u]	Relative deviation, δ [%]		
			dE/dx	Organic foil	FLUKA
T1	Aluminum	500	···	0.3	1.1
T2	Aluminum	500	···	1.0	0.3
T3	Aluminum	950	···	0.2	0.9
T4	Aluminum	950	···	0.3	0.9
T5	Copper	950	0.9	···	0.5
T6	Copper	950	0.9	···	0.4
T7	Stainless steel	950	2.5	···	0.4
T8	Stainless steel	950	1.4	···	0.6

(2) uncertainty of the ^{237}U activity in individual foils, $u(a)$, and (3) uncertainty of the total ^{237}U activity induced in the target, $u(A_\Sigma)$.

Depth uncertainty.—It can be interpreted as the uncertainty of the foil position in the target that can be measured with accuracy ~0.05 mm. However, it can also be interpreted as the uncertainty describing the experimental depth resolution, because the position of the particles that stop in a given foil is uncertain within the foil thickness. In our case, the foil thickness was 100 μm (measured with relative standard uncertainty of less than 5%). Superposition of the foil-position uncertainty and the experimental depth resolution yields the combined relative standard depth uncertainty of 0.9% at the shortest range of 13 mm.

Uncertainty of the foil activity.—There are several major sources of the uncertainty of the ^{237}U activity in the individual foils. The sources listed below were included in our uncertainty analysis.

(a) Uncertainty of the net peak area.—This uncertainty is indicated directly by Genie 2000 and GammaVision-32 and depends on the statistics in the peak (i.e. on the count rate). The relative standard uncertainty of the net peak area ranged from 0.5% for high count rates to 40% for very low count-rates.

(b) Uncertainty of the detector efficiency calibration.—This uncertainty includes: (I) the uncertainty of the calibration source activities, (II) the uncertainty of the net peak area of the calibration sources gamma lines, and (III) uncertainty of fitting of the efficiency calibration curve. The activities of the calibration sources have a certified relative standard uncertainty less than 2%. The relative standard uncertainty of the net-peak area of the calibration sources gamma lines is assumed to be less than 0.5%. The relative standard uncertainty of the efficiency calibration curve is assumed to be 1% for the gamma-ray energy 208 keV corresponding to the ^{237}U. The above values are also indicated using Genie 2000 and GammaVision-32.

(c) Uncertainty of the half-live.—The relative standard uncertainty of the ^{237}U half-live is 0.15% [10].

(d) Uncertainty of the gamma-ray emission probability per decay.—The relative standard uncertainty of the gamma-ray emission probability for 208 keV energy line of ^{237}U is 1.4% [10].

Uncertainty of the total activity.—The total activity of the ^{237}U induced in the whole target is given as a sum of individual foil activities. Its relative standard uncertainty is below 1.6% for all targets.

Uncertainty of the range.—The standard uncertainty of the range [Eq. (8)] is represented by the combined standard uncertainty, $u(R)$, of three (uncorrelated) components $u(d)$, $u(a)$, and $u(A_\Sigma)$:

$$u(R) = \sqrt{\left(\frac{\partial R}{\partial d}\right)^2 u(d)^2 + \left(\frac{\partial R}{\partial a}\right)^2 u(a)^2 + \left(\frac{\partial R}{\partial A_\Sigma}\right)^2 u(A_\Sigma)^2}. \tag{11}$$

The resulting value of the relative standard uncertainty of the range is below 3% for all targets.

It must be noted that this uncertainty, which represents the conservative assessment of the experimental uncertainty, can be further reduced. Our experiment has a "-proof-of-concept" ambition and has not been optimized yet for the best possible accuracy. More specifically, the depth resolution can be improved using thinner activation foils in the range area. The activity uncertainties can be reduced using longer irradiation time and longer measurement time of the samples. Higher count rates would lead to higher accuracy of the gamma-spectroscopy analysis. In addition, it must also be stressed that the physical accuracy limit (natural range straggling in the target) of this technique is better than, for example, in the case of tracing the β^+ emitters [11,12]. This shows the application potential of the presented technique.

V. DISCUSSION AND APPLICATIONS OF THE RESULTS

A. Validation of the FLUKA code

Comparison of the experimental depth profiles of the ^{237}U residual activity with the FLUKA simulations is presented in Fig. 5. It can be seen that the measured profiles are slightly wider than the simulated ones. This might be

influenced partly by the limited depth resolution of the experiment. The peak positions of the measured and the simulated depth profiles are approximately at the same depth in the targets T2, T5, T6, and T7. For the targets T1, T3, and T4, the simulated profiles are located deeper compared with the measured ones. In the target T8, the situation is opposite. However, in both cases, the offset is within the experimental uncertainty of the range. It can be also seen that FLUKA underestimates the total activity of ^{237}U. The ratio of the experimentally measured total activity to the total activity calculated by FLUKA varies between 1.1 and 1.5, which is still reasonable agreement keeping in mind the complexity of the fragmentation process.

Stopping power models have been significantly improved in the new version of FLUKA2011.2 in comparison with the old version of FLUKA2008.3. Barkas, Bloch, and Mott corrections as well as nuclear stopping power have been implemented in FLUKA2011.2 [35]. Thanks to these improvements, stopping powers and ranges calculated using FLUKA2011.2 are more accurate particularly for heavy ions. It is confirmed by comparison of the FLUKA simulations presented in this paper with the data published in Ref. [36]. Deviation of the ^{238}U range calculated with the FLUKA2008.3 from the experimental ones [15] is 9.2% and 7.4% for copper and stainless steel, respectively. Deviation of the ^{238}U range calculated with the new version FLUKA2011.2 from the experimental ones is 0.5% and 2.0% for copper and stainless steel, respectively.

B. Further potential of the depth-profiling range-verification technique

Although this paper deals in details with depth profiling of one particular nuclide, it should be noted that depth profiling of residual activity of other fragments can also yield information about the range of the primary beam. This is illustrated in Fig. 6 showing the depth profiles of selected fragments of the primary ions in copper irradiated with ^{238}U beam with the initial energy 500 MeV/u. The data originates from one of our previous experiments [2].

It is the position of the depth profile's front edge that coincides with the projectile range. Projectile fragments with lower proton number Z (compared to the projectile) have, in general, ranges longer than the projectiles because of the A/Z^2 dependence. However, if the fragmentation event occurs at the very end of the projectile trajectory, even these fragments do stop close to the range of the projectiles. This is the position where the depth profiles of all projectile fragments start. If the fragmentation event occurs at the target surface, the lighter fragments stop beyond the range of the primary beam. This is the position where the depth profile of the fragment ends. The lighter the fragment, the broader is its depth profile. ^{237}U is a special fragment having: (1) the proton number identical to the projectile one and (2) the mass number as close as possible to the projectile. Therefore, its depth profile is extremely narrow and follows closely the range distribution of the primary-beam particles. In the first experiment

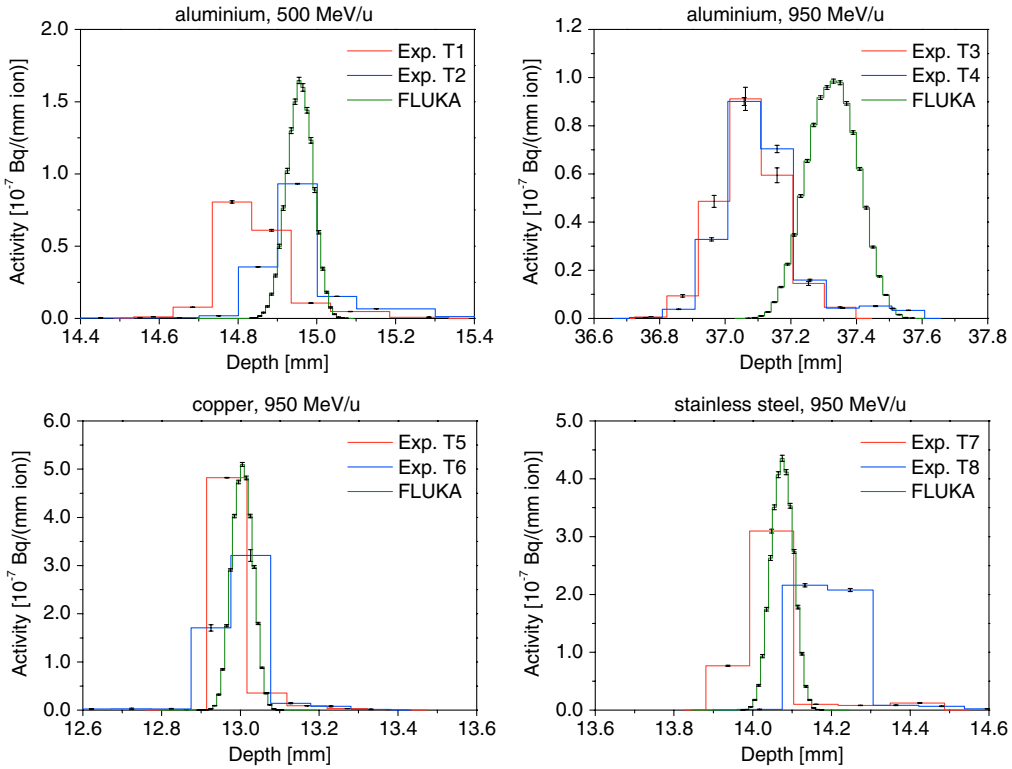

FIG. 5. Depth profiles of the ^{237}U residual activity measured experimentally and simulated by FLUKA2011.2.3 in aluminum, copper, and stainless-steel targets irradiated with ^{238}U primary ions with the initial energy 500 and 950 MeV/u.

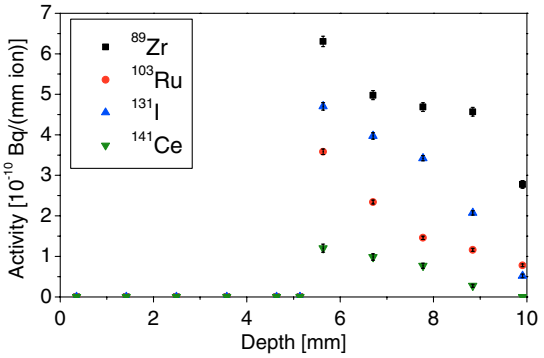

FIG. 6. Depth profiles of selected fragments of ^{238}U beam with the initial energy 500 MeV/u in copper [2].

[2], ^{237}U was detected in a single activation foil only located at the range of the primary beam. The present study is an extension of this preliminary experiment with enhanced depth resolution (a "zoom" of the range region), three target materials, two different beam energies, and more simulation codes.

There are also other suitable candidates like ^{196}Au (half-life 6.183 days) and ^{195}Au (half-life 186.09 days) to verify the range of the ^{197}Au beam. It should also be noted that similar experiments could be done with radioactive beams, but we concentrate on beams of stable nuclei that can be "traced" by their own fragments produced directly in the target. Furthermore, we concentrate on fragments that are gamma emitters and can be analyzed by a standard gamma-spectrometry chain.

VI. SUMMARY AND CONCLUSIONS

Aluminum, copper and stainless-steel targets were irradiated with ^{238}U beam with the initial energy 500 and 950 MeV/u and analyzed using gamma-ray spectroscopy. The stacked-foil target geometry allowed for depth profiling of the residual activity of ^{237}U. The ^{237}U is a fragment of the ^{238}U primary ion. On the basis of the depth-profiling measurements, the range and the range straggling of ^{237}U were calculated. Since the range of heavy ions is proportional to A/Z^2, the signal from the ^{237}U can be used for the range verification of the ^{238}U primary ions. The offset between ^{237}U and ^{238}U ranges is within the experimental uncertainty, which was shown using computer codes ATIMA, SRIM (both without inelastic nuclear interactions) and FLUKA (including inelastic nuclear interactions). As expected, the range of the ^{237}U is shorter than the range of the ^{238}U, but the difference is below 0.5%. This also indicates that the inelastic nuclear interaction $^{238}\text{U} \rightarrow {}^{237}\text{U}$ (fragmentation event) has a negligible influence on the energy loss and change of momentum of the ^{237}U fragment with respect to its ^{238}U parent.

The range straggling of the ^{237}U fragments calculated by FLUKA is wider than the range straggling of the ^{238}U primary ions by factor of from about 1.5 to 2. This is caused by the fact that the fragmentation events occur at different depths of the target.

The results obtained using the depth-profiling technique were compared with complementary dE/dx and organic-foil experiments. The comparison showed an agreement within 2.5% (the largest deviation, single case only), but most values were below 1% (see Table VI).

The data collected in this paper also show that the total induced activity of the ^{237}U in a target is increasing with increasing proton number of the target material (data available for aluminum, copper, and stainless steel). It is also increasing with increasing energy of the primary beam in the range from hundreds of MeV/u to 1 GeV/u. It is due to the EMD process that becomes important especially for nuclear interaction of high-energy heavy ions with high-Z target materials.

It was found out that FLUKA underestimates the total activity of ^{237}U by a factor of 1.1 to 1.5 and the straggling of the experimental depth profiles is wider than the straggling of the simulated ones. This may be caused by the limited depth resolution of the experiment.

The paper demonstrated feasibility of using depth profiling of residual activity as a range-verification technique for primary beams, in general. The in-depth study was performed for the particular case of ^{237}U as a range-verifying fragment of ^{238}U primary beam.

[1] FAIR—Baseline Technical Report (GSI Darmstadt, Germany, 2006).
[2] A. Fertman *et al.*, Nucl. Instrum. Methods Phys. Res., Sect. B **260**, 579 (2007).
[3] I. Strašík *et al.*, Nucl. Instrum. Methods Phys. Res., Sect. B **266**, 3443 (2008).
[4] E. Mustafin *et al.*, Radiat. Eff. Defects Solids **164**, 460 (2009).
[5] I. Strašík, E. Mustafin, T. Seidl, and M. Pavlovič, Nucl. Instrum. Methods Phys. Res., Sect. B **268**, 573 (2010).
[6] V. Chetvertkova *et al.*, Nucl. Instrum. Methods Phys. Res., Sect. B **269**, 1336 (2011).
[7] I. Strašík *et al.*, Nuclear Technology **168**, 643 (2009) [http://www.new.ans.org/pubs/journals/nt/a_9282].
[8] E. Kozlova *et al.*, Nuclear Technology **168**, 747 (2009) [http://www.new.ans.org/pubs/journals/nt/a_9300].
[9] I. Strašík, E. Mustafin, and M. Pavlovič, Phys. Rev. ST Accel. Beams **13**, 071004 (2010).
[10] R. B. Firestone and L. P. Ekström, LBNL Isotopes Project—LUNDS Universitet, WWW Table of radioactive isotopes, [http://ie.lbl.gov/toi/].
[11] W. Enghardt *et al.*, Nucl. Instrum. Methods Phys. Res., Sect. A **525**, 284 (2004).
[12] K. Parodi *et al.*, Nucl. Instrum. Methods Phys. Res., Sect. A **591**, 282 (2008).
[13] A. Fertman *et al.*, GSI Report No. 2007-2 EP-16, 2007 [https://www.gsi.de/informationen/wti/library/plasma2006/PAPERS/EP-16.pdf].

[14] A. Fertman *et al.*, in *Proceedings of the International Topical Meeting on Nuclear Research Applications and Utilization of Accelerators, Vienna, Austria, 2009* (IAEA, Vienna, Austria, 2010), AT/P5-09.
[15] A. A. Golubev *et al.*, Nucl. Instrum. Methods Phys. Res., Sect. B **263**, 339 (2007).
[16] V. Chetvertkova *et al.*, in *Proceedings of the 46th ICFA Advanced Beam Dynamics Workshop on High-Intensity and High-Brightness Hadron Beams HB2010, Morschach, Switzerland, 2010* (PSI, Viligen, Switzerland, 2011), p. 250.
[17] E. Mustafin, I. Strašík, and T. Seidl, GSI Report, GDS-ID: DOC-2009-Apr-89, (2009) [https://www.gsi.de/documents/DOC-2009-Apr-89-1.pdf].
[18] G. Battistoni *et al.*, in *Proceedings of the Hadronic Shower Simulation Workshop, Fermilab, Batavia, Illinois, USA, 2006*, AIP Conf. Proc. No. 896 (AIP, Melville, New York, 2007), p. 31.
[19] A. Ferrari, P. R. Sala, A. Fasso, and J. Ranft, Reports No. CERN-2005-10, INFN/TC_05/11, and SLAC-R-773.
[20] 11th Fluka Course, Prague, Czech Republic, 2011 [www.fluka.org].
[21] J. F. Ziegler, J. P.Biersack, and M. D. Ziegler, in *SRIM–The Stopping and Range of Ions in Matter* (Lulu Press Co., Morrisville, NC, 2008), SRIM code available from http://www.srim.org.
[22] J. F. Ziegler, M. D.Ziegler, and J. P. Biersack, Nucl. Instrum. Methods Phys. Res., Sect. B **268**, 1818 (2010).
[23] http://www-linux.gsi.de/~weick/atima.
[24] H. Reeg and N. Schneider, in *Proceedings of the Fifth European Workshop on Diagnostics and Beam Instrumentation DIPAC2001, ESRF, Grenoble, France, 2001* (ESRF, Grenoble, France, 2001), PS08.
[25] B. Jurado, K. H. Schmidt, and K. H. Behr, Nucl. Instrum. Methods Phys. Res., Sect. A **483**, 603 (2002).
[26] J. Lindhard and A. H. Soerensen, Phys. Rev. A **53**, 2443 (1996).
[27] J. F. Ziegler, J. B. Biersack, and U. Littmark, in *The Stopping and Range of Ions in Solids* (Pergamon Press, New York, 1985), Vol. 1.
[28] W. Brandt and M. Kitagawa, Phys. Rev. B **25** 5631 (1982).
[29] J. W. Norbury, Phys. Rev. C **47**, 406 (1993).
[30] J. W. Norbury, Phys. Rev. C **42**, 2259 (1990).
[31] J. W. Norbury and A. Adamczyk, Nucl. Instrum. Methods Phys. Res., Sect. B **254**, 177 (2007).
[32] H. Paul, Nucl. Instrum. Methods Phys. Res., Sect. B **268**, 3421 (2010).
[33] E. Mustafin, I. Hofmann, and H. Weick, Nucl. Instrum. Methods Phys. Res., Sect. A **501**, 553 (2003).
[34] Joint Committee for Guides in Metrology (JCGM), in Evaluation of Measurement Data–Guide to the Expression of Uncertainty in Measurement (JCGM, 2008).
[35] FLUKA Team 2000–2012, Release notes for FLUKA2011.2 [www.fluka.org].
[36] V. Chetvertkova *et al.*, in *Proceedings of the 10th Workshop on Shielding Aspects of Accelerators, Targets and Irradiation Facilities SATIF10, CERN, Geneva, Switzerland, 2010* (NEA OECD Publishing, Paris, France, 2011), p. 249.